High-pressure, halogen-bearing melt preserved in ultrahigh-temperature felsic granulites of the Central Maine Terrane, Connecticut (U.S.A.)

SILVIO FERRERO^{1,2,*,†}, JAY J. AGUE³, PATRICK J. O'BRIEN¹, BERND WUNDER⁴, LAURENT REMUSAT⁵, MARTIN A. ZIEMANN¹, AND JENNIFER AXLER⁶

¹Institut für Geowissenschaften, Universität Potsdam, Karl-Liebknecht-Str. 24-25, 14476 Potsdam-Golm, Germany
²Museum für Naturkunde (MfN), Leibniz-Institut für Evolutions-und Biodiversitätsforschung, 10115 Berlin, Germany
³Department of Earth and Planetary Sciences, Yale University, 210 Whitney Avenue, New Haven, Connecticut 06511, U.S.A.
⁴Helmholtz-Zentrum Potsdam, GFZ, D-14473 Potsdam, Germany

⁵Museum National d'Histoire Naturelle, 7C Rue Guy de la Brosse, 75005 Paris, France ⁶Department of Geosciences, Science Center, Wellesley College, 106 Central Street, Wellesley, Massachusetts 02481, U.S.A.

ABSTRACT

Inclusions of relic high-pressure melts provide crucial information on the fate of crustal rocks in the deep roots of orogens during collision and crustal thickening, including at extreme temperature conditions exceeding 1000 °C. However, discoveries of high-pressure melt inclusions are still a relative rarity among case studies of inclusions in metamorphic minerals. Here we present the results of experimental and microchemical investigations of nanogranitoids in garnets from the felsic granulites of the Central Maine Terrane (Connecticut, U.S.A.). Their successful experimental re-homogenization at ~2 GPa confirms that they originally were trapped portions of deep melts and makes them the first direct evidence of high pressure during peak metamorphism and melting for these felsic granulites. The trapped melt has a hydrous, granitic, and peraluminous character typical of crustal melts from metapelites. This melt is higher in mafic components (FeO and MgO) than most of the nanogranitoids investigated previously, likely the result of the extreme melting temperatures—well above 1000 °C. This is the first natural evidence of the positive correlation between temperature and mafic character of the melt; a trend previously supported only by experimental evidence. Moreover, it poses a severe caveat against the common assumption that partial melts from metasediments at depth are always leucogranitic in composition.

NanoSIMS measurement on re-homogenized inclusions show significant amounts of CO₂, Cl, and F. Halogen abundance in the melt is considered to be a proxy for the presence of brines (strongly saline fluids) at depth. Brines are known to shift the melting temperatures of the system toward higher values and may have been responsible for delaying melt production via biotite dehydration melting until these rocks reached extreme temperatures of more than 1000 °C, rather than 800–850 °C as commonly observed for these reactions.

Keywords: High-pressure granulites, anatexis, nanogranitoids, carbon, halogens, piston cylinder; High-Grade Metamorphism, Anatexis, and Granite Magmatism

Introduction

The investigation of melt inclusions in felsic (Ferrero et al. 2015; Cesare et al. 2015) and mafic (Ferrero et al. 2018a) granulites is the most straightforward approach to the investigation of melting processes in the lower continental crust, directly in their source region. These droplets of anatectic melt are generally partially to totally crystallized, i.e., as nanogranitoids, due to the slow cooling of the host rock (Ferrero et al. 2012; Cesare et al. 2015). They contain a cryptocrystalline aggregate of phases consistent with the crystallization of a silicate-rich melt (Ferrero et al. 2018b). The expected phases include, but are not limited to, OH-bearing phases, quartz, and feldspar(s), or their metastable polymorphs (Ferrero et al. 2016b). Just like fluid

and mineral inclusions, melt inclusions in metamorphic rocks are tools for natural scientists to peer into the history of the host rocks, obtain geochemical information on deep processes, and to better constrain *P-T-t-X* evolution (Ferrero and Angel 2018).

Multiphase inclusions with features consistent with nanogranitoids were reported by Axler and Ague (2015) in garnets from layers of sillimanite-rich rocks hosted in gneisses of the Central Maine Terrane (CMT, Acadian orogeny, northeast Connecticut, U.S.A.). Phase assemblages in the inclusions and microstructures classify them as former droplets of melt trapped during garnet formation at the metamorphic peak $\sim 1050~^{\circ}\text{C}$ and $\geq 1~^{\circ}\text{C}$ (Axler and Ague 2015). The host rock has attracted considerable interest in recent years because of its very high T of re-equilibration at relatively low P (including cordierite-spinel assemblages), allowing Ague et al. (2013) to interpret them as the first example of ultrahigh temperature (UHT) metamorphic rocks in North America. By definition, UHT metamorphism involves

^{*} E-mail: sferrero@uni-potsdam.de. Orcid 0000-0002-9948-3676

[†] Special collection papers can be found online at http://www.minsocam.org/MSA/AmMin/special-collections.html.

T in excess of 900 °C achieved along the apparent geothermal gradient ≥20 °C/km (Brown 2006), i.e., mostly in the stability field of sillimanite. UHT metamorphism has been to date identified in dozens of localities worldwide, mostly in Precambrian rocks (Kelsey 2008), although much younger UHT rocks, i.e., Miocene in age, have also been recently reported (Pownall et al. 2018). More recent studies of other rocks in the CMT document high-pressure granulite facies metamorphism (~1050 °C, ~1.8 GPa) of silica-undersaturated garnet-spinel-corundum gneisses (Keller and Ague 2018), as well as UHP metamorphism (Keller and Ague 2020).

Piston-cylinder re-homogenization followed by in situ characterization is a common and well-established approach for nanogranitoid studies to follow to (1) prove that they originally were indeed droplets of melt and (2) characterize geochemistry and fluid content and speciation content of anatectic melt (e.g., Acosta-Vigil et al. 2016; Bartoli et al. 2016, 2019; Carvalho et al. 2019). Our detailed experimental and microchemical work confirmed that the CMT multiphase inclusions were originally a hydrous and halogen-rich granitic melt formed at *T* in excess of 1000 °C, the hottest preserved melt so far found in natural metasedimentary protolith. Our approach leads to surprising outcomes with broad significance in terms of melt composition and melting processes in the deepest parts of orogenic root zones, as well as of regional geodynamic evolution.

METHODS

Our study used a piston-cylinder press, backscattered-electron (BSE) imaging, electron probe analyses (EPMA), energy-dispersive spectrometry (EDS) elemental mapping, and micro-Raman spectroscopy. Several garnet chips with unexposed nanogranitoids of both equant and tubular shape were manually separated from doubly polished thick sections and used as starting material in re-homogenization experiments. The chips were loaded in platinum capsules of 4 mm length, 3 mm diameter, and cold-sealed after filling. Four or five chips were used per each experiment, depending on the size of the chips. Powdered silica was added in the capsule to isolate the chips both from each other and from the capsule walls, and no water was added to the experimental charge. The pressure cells consisted of talc-pyrex glass outer sleeves with graphite furnace and crushable alumina inner spacers in which the Pt-capsule was embedded [for more details on the experimental setup, see Bartoli et al. (2013a), Cesare et al. (2015), and repository data of Ferrero et al. (2015)]. The assemblage was then kept in a Johannes-type piston-cylinder apparatus at GFZ-Potsdam at variable T and P conditions for up to 24 h. The temperature (T) in the capsule was controlled using a Type S thermocouple (Pt-PtRh10) with a ±10 °C uncertainty. The assemblage has been pressure calibrated via the equilibrium quartz-coesite according to Mirwald and Massonne (1980), which is accurate within 50 MPa. Quenching of the experimental charge took place at high P, and the machine was unloaded only after reaching ambient T. In situ analyses were then performed on capsules mounted in epoxy and polished to expose re-homogenized inclusions (for further details see Bartoli et al. 2013a; Ferrero et al. 2015).

The field emission gun electron microprobe (FEG-EMP) JEOL Hyperprobe JXA-8500F available at the Natural History Museum of Berlin was used to acquire high-resolution BSE images and EDS elemental maps on nanogranitoids and re-homogenized inclusions. The glass resulting from re-homogenization was analyzed using a JEOL JXA-8200 EMP at Potsdam University. Analytical conditions were similar to previous studies of nanogranitoids (Ferrero et al. 2012, 2015) at 15 kV, 3.5 nA, and beam diameter of 1 µm to avoid contamination from the surrounding host. Alkali loss correction factors were estimated using haplogranitic standards (Morgan and London 2005) and are in the range 17–23% relative for Na₂O and 10–13% relative for K₂O depending on the analytical session.

Fluorine, CO₂, and H₂O analyses were performed via Nano Secondary Ion Mass Spectrometry (NanoSIMS) using the Cameca NanoSIMS 50 operated at the Muséum National d'Histoire Naturelle of Paris following the procedure described in Bartoli et al. (2014) and Créon et al. (2018). Polished capsules with re-homogenized inclusions on the garnet surface were mounted in indium

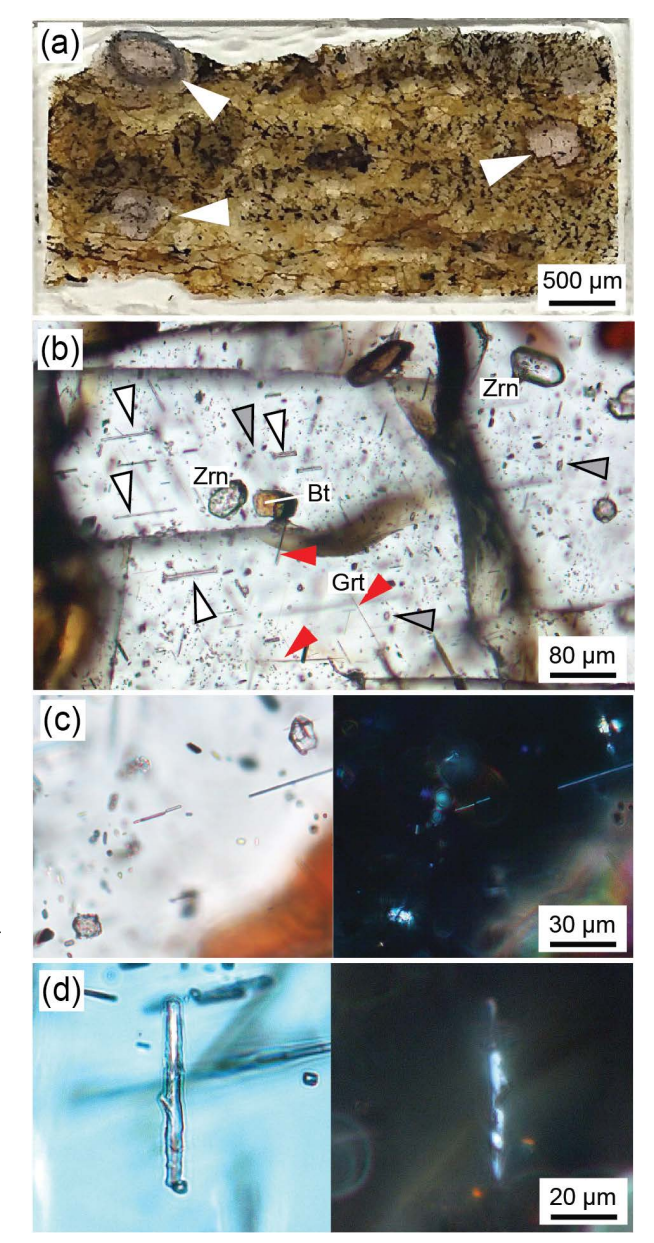


FIGURE 1. Microstructural features of inclusions and host rocks.

(a) Scan of a representative thick section with garnets in a more felsic matrix; the garnet in the upper left corner has a circle made with a black marker. White arrows = MI-bearing garnets. Sample JAQ-124A.

(b) Cluster of polycrystalline inclusions occurring in the center of the garnet, mineral abbreviations from Whitney and Evans (2010). White arrows = needle-shaped nanogranitoids. Gray arrows = isometric nanogranitoids, generally smaller than the first inclusion type. Red arrows = thin rutile needles. (c) Close-up of isometric nanogranitoids (left) with multiple birefringent phases visible under crossed polars (right).

(d) Close-up of a needle-shaped nanogranitoid (left), occasionally with the rough outline already described by Axler and Ague (2015), and showing once again several birefringent phases under crossed polars (right).

along with standard glasses, and the inclusions were identified through images of $^{28}\text{Si}^-$ and $^{56}\text{Fe}^{16}\text{O}^-$ secondary ions. Pre-sputtering on a $5\times5~\mu\text{m}^2$ surface area for 2 min preceded each analysis to remove the gold coating, surface contamination, and achieve a steady-state sputtering regime (Thomen et al. 2014). A 20 pA Cs⁺

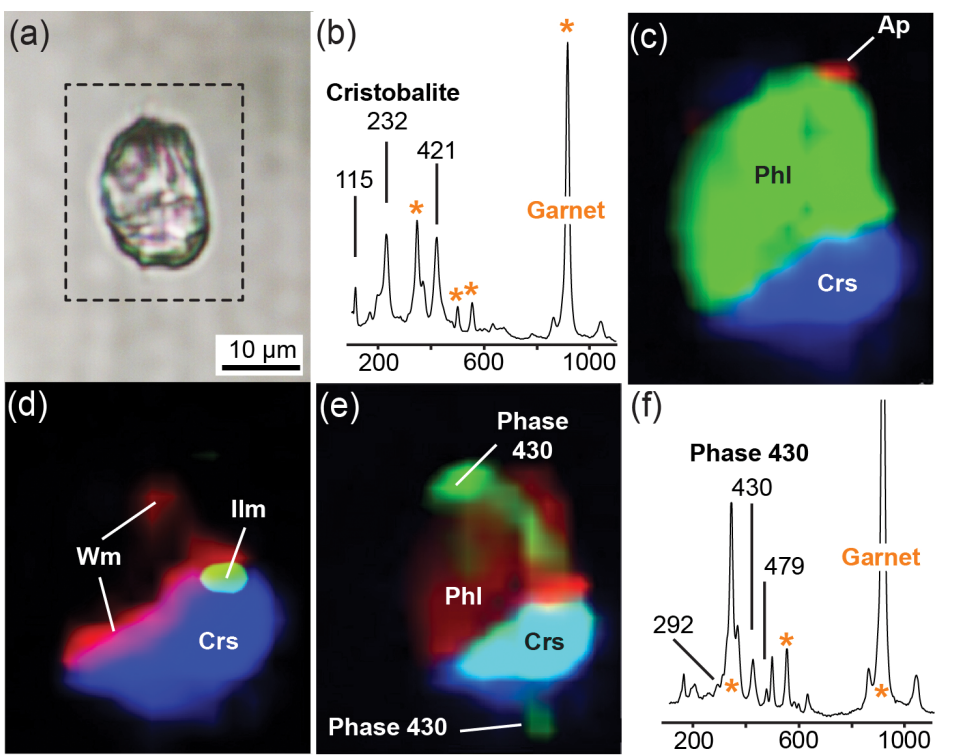


FIGURE 2. Results of MicroRaman investigation of a representative inclusion below the surface (a). (b) Raman spectrum of cristobalite from the CMT nanogranitoids. (c) The map shows the distribution of Raman peak 415 cm⁻¹ of cristobalite (blue), 196 cm⁻¹ of phlogopite (green), and 963 cm⁻¹ of apatite (red). Also in **d**, the distribution of peak 707 of white mica (red) and the 675 cm⁻¹ peak of ilmenite (green) are visible. In e, the distribution of peak 430 cm⁻¹ is visible in green, whereas a representative spectrum of phase 430 is reported in f.

primary beam was used for data acquisition via rastering of a $3 \times 3 \mu m^2$ surface area. Ions were exclusively collected from the inner $1 \times 1 \mu m^2$ (using the beam blanking mode) to minimize surface contamination. Each analysis comprised 200 cycles with a duration of 1.024 s. Secondary ions of 12C-, 16OH- (proxy for H₂O), ¹⁹F-, ²⁸Si-, and ⁵⁶Fe¹⁶O- were recorded simultaneously in multicollection mode, using electron multipliers with a dead time of 44 ns. Mass resolution was set to 5500 to resolve any mass interference on the selected ions. Only analyses with a stable 16OH-/28Si- ratio were considered in this study. Three glasses of leucogranitic composition and known concentrations of H2O, varying between ~0.3 and 4.86 wt% were used for calibration (Bartoli et al. 2014; see also Online Material1). For F concentration, we used NIST 610 and 612 standards to determine [F]/[SiO₂] ratios from ¹⁹F^{-/28}Si⁻ (Hauri et al. 2002). Four trachyandesitic standards (STR 9, 10, 11, and 13) were used to correct for carbon measurements (Créon et al. 2018): these are glass fragments of shoshonite lava from the Stromboli volcano that were experimentally doped in carbon and water by Bureau et al. (2003). Analytical uncertainty on each NanoSIMS measurement (based on the Poisson error due to counting statistics) was combined with the uncertainty on the calibration (corresponding to 66% interval of confidence) by quadratic sum to obtain the 66% uncertainty on values reported in Online Material Table OM1.

Micro-Raman spectroscopy was performed using a HORIBA Jobin Yvon LabRAM HR 800 located at the Institute of Geoscience, University of Potsdam. An air-cooled Nd:YAG laser was used for excitation ($\lambda = 532$ nm, laser power on the sample of 2-3 mW) with a grating of 300 lines/mm, slit width, and confocal hole set to 100 and 200 µm, respectively. The Raman spectra of re-homogenized glass inclusions, as well as crystal phases, were acquired with a 100× objective in the wavenumber range $100\text{--}4000~\text{cm}^{-1}$, integrating 3 repetitions of 30~s with spectral resolution of 10 cm⁻¹. The Raman map was acquired using a spot diameter of 1–1.5 μ m and consists of a grid of 19 \times 22 points separated by 0.7 μ m. Each spectrum was obtained integrating 2 repetitions of 30 s in 4 spectral windows. The software LabSpec 6.0 was used for spectral processing. The inclusion was mapped at ~5 um depth, causing the spectra to be superimposed by strong Raman bands of the garnet host. The complete garnet spectrum was removed with an adopted peak intensity of the most intense garnet band at each point of the map, to improve the visibility of the spectra of the mineral phases. Few points showed luminescence, which was then removed via background subtraction. Different phases were visualized in the map by color coding of the indexed Raman bands of the phases (cf. O'Brien and Ziemann 2008).

PETROGRAPHIC FEATURES OF THE STARTING MATERIAL

The host rocks are rusty schists characterized by the assemblage garnet+sillimanite+K-feldspar+plagioclase+quartz+ cordierite+biotite (Fig. 1a). The sillimanite is commonly found as pseudomorphs after kyanite. Detailed information on sample location and petrographic features are in Axler and Ague (2015). The inclusions occur in the inner part of garnet porphyroblasts with a random distribution indicative of a primary nature, i.e., entrapment during growth of the host garnet (Fig. 1b; see also Ferrero et al. 2012). They vary in shape from isometric with diameter ≤10 µm (Fig. 1c) to needles with length ≤100 µm and few micrometers across (Fig. 1d). The latter type is by far the most common in each cluster, a shape never before observed in such abundance in case studies of nanogranitoid, which are more commonly isometric (Ferrero et al. 2018b; Cesare et al. 2015). The most elongated inclusions often show cracks of limited extension at the corners, evidence of decrepitation. The detailed microchemical and microstructural investigation of the inclusions performed by Axler and Ague (2015) showed that, before the experimental runs, they contain a constant assemblage consisting of quartz, phlogopite, white mica and, very often, a compositionally variable phase (CV phase in Axler and Ague 2015) interpreted as residual glass or its nanocrystalline breakdown product.

Raman investigation (Fig. 2a) and mapping of isometric inclusions show that cristobalite is present instead of quartz in some inclusions (Fig. 2b) and coexists with two micas and accessory phases such as apatite and ilmenite (Figs. 2c–2e), whereas no inclusions show the presence of residual glass. However, the Raman map shows a crystalline phase with main peaks at 292,

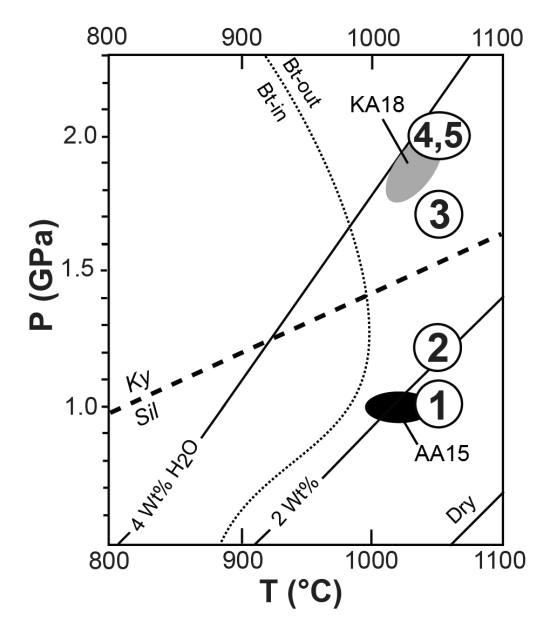


FIGURE 3. Experimental conditions (numbers in circles) vs. previous estimates of metamorphic peak equilibration for the host gneisses of the investigated nanogranitoids. Solid lines: liquidus curves for different amount of $\rm H_2O$ according to Johannes and Holtz (1996). AA15 = T and minimum P conditions proposed by Axler and Ague (2015) for the felsic granulites investigated in the present study. KA18 = HP conditions estimated on garnet-spinel-corundum gneisses of the Central Maine Terrane by Keller and Ague (2018). Experiments 4 and 5 were conducted at the same conditions with different durations (see Table 1).

430, and 479 cm⁻¹, assigned to a still unidentified and possibly new phase (hence "phase 430") already found and analyzed in nanogranitoids from HP/UHP rocks of the Bohemian Massif (unpublished data), and having a composition similar to a granitic glass. Graphite occurs as mineral inclusions in garnet and occasionally as a trapped phase in the inclusions. A prominent feature of the host garnet is the presence of abundant rutile and ilmenite needles dominantly oriented parallel to <111> of garnet. Interestingly, needle-shaped nanogranitoids are oriented in the same directions, and may contain rutile or, very rarely, ilmenite as trapped phases (Axler and Ague 2015).

RESULTS

Five re-homogenization experiments were performed at $T=1050~^{\circ}\mathrm{C}$ and variable confining P in the range 1.0–2.0 GPa (details on experimental runs and products are in Table 1; P-T conditions of each experiment are summarized in Fig. 3). The experimental conditions were chosen to be as close as possible to the conditions of formation, estimated to be $\approx 1040~^{\circ}\mathrm{C}$ based on Zr-in-Rt thermometry (Tomkins et al. 2007) on the rutile needles present along with nanogranitoids in the garnet core (Axler and

Ague 2015). The T estimates were calculated assuming 1 GPa as formation P of the host garnet and melt entrapment, thus representing a minimum value (Ague et al. 2013).

Each experiment shows complete re-melting of the inclusions, i.e., no leftovers of the original phases in the nanogranitoids are visible after the heating run, with the exception of clearly trapped accessories such as rutile and ilmenite. The absence of embayments and the presence of regular linear walls in the inclusions rules out that garnet dissolved into the melt (Ferrero et al. 2012; Bartoli et al. 2013b), as expected in case of significant overheating during the experiments, i.e., the chosen T is likely very close to the liquidus of the trapped melt. However, the experiments performed at P < 1.7 GPa (numbers 1 and 2 in Fig. 3) constantly show formation of new garnet, higher in Mg than the original host phase (Figs. 4a-4d) and occasionally small orthopyroxene crystals identified via Raman spectroscopy at $P \le 1.2$ GPa. Moreover, at 1 GPa most inclusions show extensive evidence of decrepitation (Fig. 4a). The three experiments performed at 1.7 and 2.0 GPa (numbers 3, 4, and 5, Fig. 3) do show fully rehomogenized glassy inclusions without evidence of decrepitation and/or formation of new phases (Figs. 4e-4i).

Melt composition

The glass measured in 19 inclusions (Table 2) after successful experimental re-homogenization is hydrous, granitic (Figs. 5a and 5b) and very K-rich (avg. $K_2O/Na_2O = 3.90$, Table 2), with a clear peraluminous (ASI = 1.22, Fig. 5c) and alkalic to alkalicalcic character (Fig. 5d). Importantly, such melts are not leucogranitic, as commonly expected for anatectic melts from melting of metasediments: they have indeed a high-FeO+MgO content (4.05 wt%; 4.25 wt% when recalculated on an anhydrous basis; Table 2). The presence of H_2O in the glass is visible in Raman spectra acquired on re-homogenized nanogranitoids, which show the broadband of water in the region $3200-3800 \, \mathrm{cm}^{-1}$ (Fig. 6).

The H₂O content of the melt, along with CO₂ and F, was measured in garnets from experiments 3 and 4 using NanoSIMS. One single inclusion shows very low values of all three volatile species, suggesting that it may have lost most of its volatiles, possibly as a result of decrepitation during quenching (measurement Exp3 MI 1 in Table 3), and thus it is not further considered in the average values calculated below. The volatiles were quantified as 4.40 wt% H₂O, 3072 ppm CO₂, and 3161 ppm F on average (Fig. 7a). With the exclusion of the single analysis discussed above, H2O content in the rest of the data set is consistent (Fig. 7a), whereas the CO₂ and F contents of the melt vary by an order of magnitude (Fig. 7a; Table 3) depending on the inclusion (Figs. 7b and 7c). Interestingly, EMP measurements on the re-homogenized inclusions show that Cl is also present in remarkable amounts, reaching almost 1 wt%, with average 0.32 wt%, making this melt more enriched in halogens (Cl, F) than any previous anatectic melt so far investigated in nanogranitoids.

TABLE 1. Conditions, relevant info, and results of piston-cylinder experiments

Experiment	Figures	T (°C)	P (GPa)	t (h)	Melting	Decrepitation	Melt-host interaction	Full re-homogenization
1	4a, 4b, 4c	1050	1.0	≈15	Х	X (extensive)	X (new Grt+New Opx)	_
2	4d	1050	1.2	24	Χ	-	X (new Grt)	-
3	4e, 4f, 4g, 4h	1050	1.7	24	X	-	-	X
4	4i	1050	2.0	24	Χ	-	-	X
5	-	1050	2.0	4	X	-	_	X

American Mineralogist, vol. 106, 2021

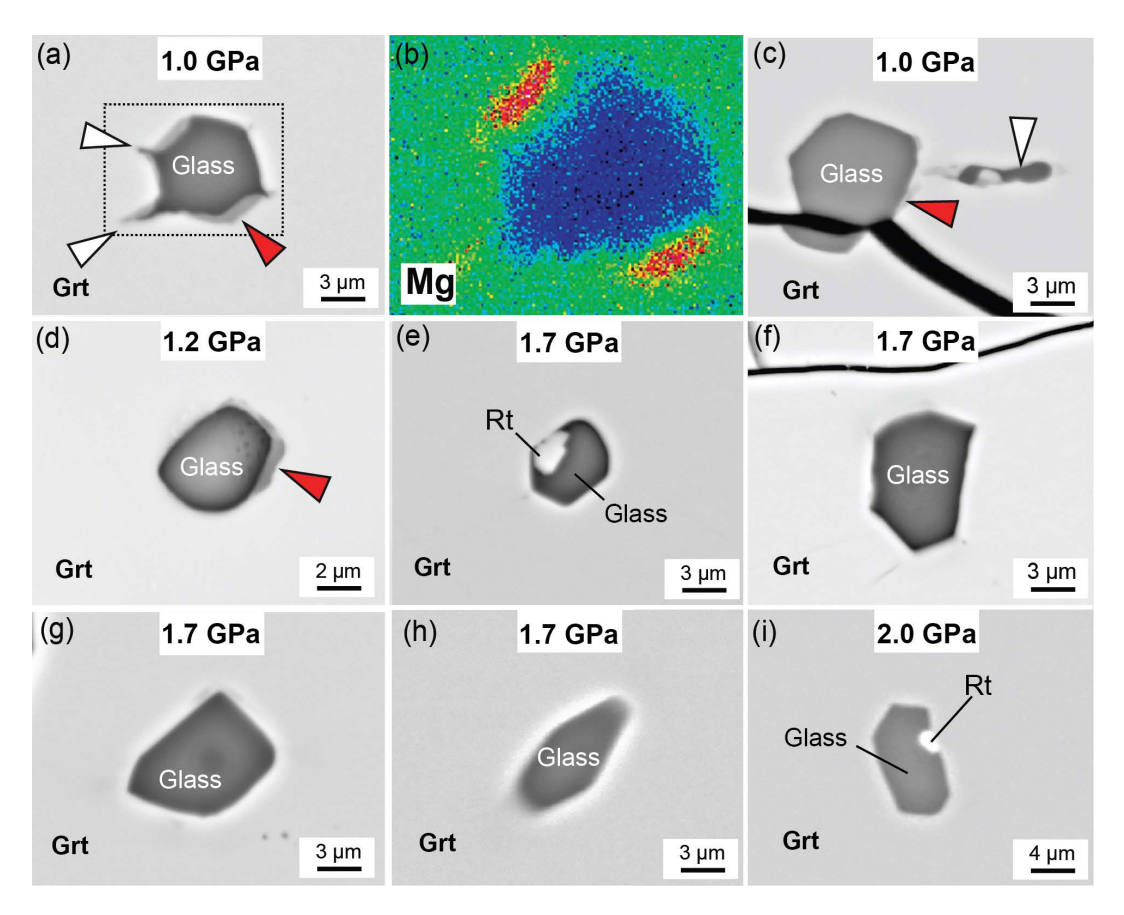


FIGURE 4. BSE images of CMT nanogranitoids after piston-cylinder experiments under different confining *P*. White arrows = decrepitation cracks. Red arrows = new Mg-richer garnet. See text for details on the single images.

FIGURE 5. Composition of re-homogenized nanogranitoids. (a) Ab-Or-Qz and (b) Ab-Or-An normative diagrams. (c) Alumina Saturation Index (ASI) = molar Al/ (Ca+Na+K) vs. Alkalinity Index (AI) = molar Al-(Na+K). (d) Silica content vs. Modified Alkali-Lime Index (MALI) = Na₂O+K₂O-CaO. CMT = central Maine Terrane; KKB = UHT nanogranites of the Kerala Khondalite Belt (Ferrero et al. 2012). P91 = experimental melts from Patiño Douce and Johnston (1991). For EMP compositions and P-T conditions of formation of the KKB and P91 melts see Table 2.

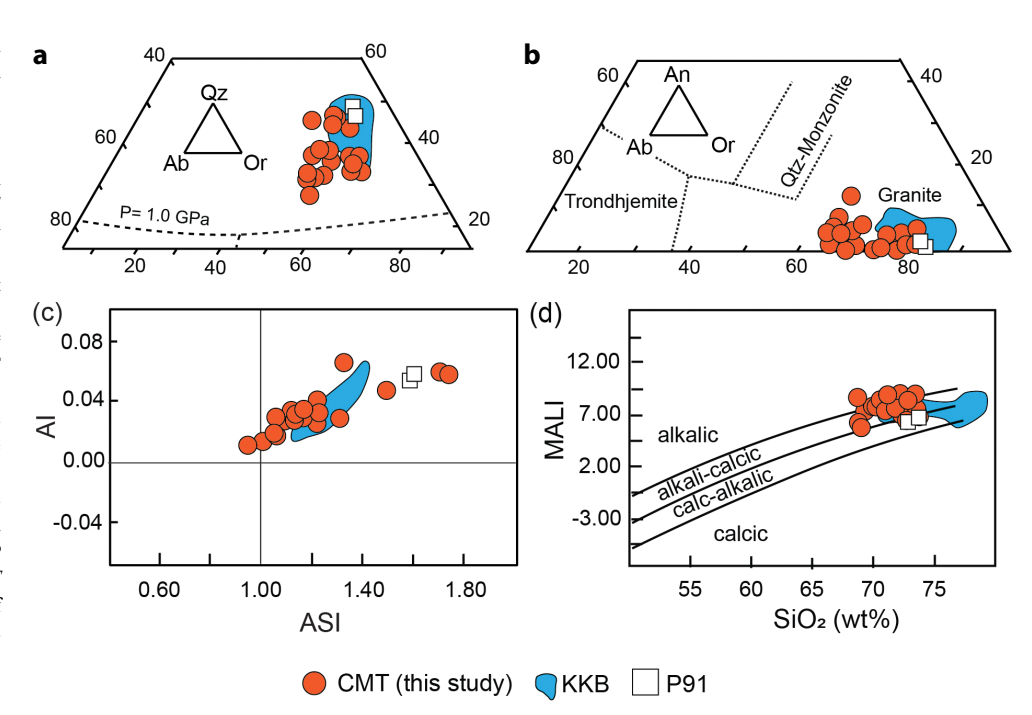


TABLE 2. Geochemistry and *P-T* conditions of formation of re-homogenized melt inclusions (n = 19) from the Central Maine Terrane, experimental melts from metasediments (P91 = Patiño-Douce and Johnston 1991) and averages of melt inclusion analyses from different case studies of metasediments melted under different conditions

									ntral M												
Name	21		av.44–4		20	21	22	23	24	7	8	32	35	34	3	6	36		21/22	Avg.	St.dev.
Duration	24 h	24 h	24 h	24 h	24 h	24 h	24 h	24 h	24 h	24 h		24 h									
T (°C)	1050	1050	1050	1050	1050	1050	1050	1050	1050	1050		1050		1050	1050	1050	1050		1050		
P (GPa)	1.7	1.7	1.7	1.7	1.7	1.7	1.7	1.7	1.7	1.7	1.7	1.7	1.7	2.0	2.0	2.0	2.0	2.0	2.0		
wt%																					
SiO ₂	64.96	68.89	63.61	67.10	69.15	68.22	67.64	66.00	68.32	66.80	67.30	70.97	70.92	68.83	71.07	68.24	71.97	71.91	66.36	68.33	(2.34)
TiO ₂	0.64	0.36	0.03	0.05	0.91	0.24	0.14	0.14	0.10	0.05	0.16	0.22	0.15	0.13	0.10	0.00	0.33	0.66	0.07	0.23	(0.25)
Al_2O_3	12.61	12.5	14.74	12.39	12.96	12.89	13.80	12.42			14.03	13.18	14.00		11.83	13.46	13.23	11.93	13.14	13.04	(0.81)
FeO	3.71	4.76	4.43	3.27	3.22	3.53	3.25	4.10	3.08	2.89	2.38	3.53	2.41	3.97	4.75	2.22	3.49		3.54	3.47	(0.74)
MnO	0.11	0.11	0.04	0.02	0.09	0.14	0.02	0.08	0.01	0.00	0.00	0.06	0.09	0.01	0.01	0.00	0.03	0.08	0.07	0.05	(0.05)
MgO	0.61	0.58	0.63	1.11	0.38	0.41	0.70	1.01	0.63	0.57	0.30	0.62	0.45	0.56	0.61	0.34	0.52	0.54		0.62	(0.20)
CaO	1.17	0.98	1.68	0.01	0.36	0.14	0.12	0.36	0.03	0.94	0.55	1.09	0.58	0.54	0.60	0.98	0.56	0.84	0.88	0.65	(0.45)
Na₂O	1.32	1.28	1.58	1.71	1.28	1.50	1.66	1.17	1.14	1.89	1.68	2.11	2.17	2.29	2.45	3.03	2.68		1.52	1.76	(0.58)
K₂O	6.93	7.00	5.11	6.10	7.23	7.17	4.71	5.23	5.51	6.01	7.41	5.81	6.68	6.18	6.07	6.69	6.51	6.45		6.26	(0.78)
P ₂ O ₅	0.59	0.75	0.28	0.05	0.18	0.15	0.16	0.12	0.07	0.23	0.19	0.17	0.07	0.07	0.00	0.12	0.25	0.20	0.38	0.21	(0.19)
CI .	0.07	0.21	0.08	0.86	0.82	0.68	0.95	0.93	0.97	0.01	0.04	0.00	0.01	0.09	0.10	0.10	0.10	0.00		0.32	(0.39)
Total	92.64	97.21	92.12	91.79	95.76	94.38	92.2	90.62	92.59	96.17	98.00	97.76	97.53	94.64	97.49	99.07	99.57	97.05	93.29	95.26	
Q	26	30	27	29	31	29	36	34	37	32	30	31	29	27	27	25	27	37	29	30	
C	2	3	4	3	3	3	6	4	6	2	2	2	2	1	0	0	1	2	3	3	
Or	41	41	30	36	43	42	28	31	33	37	45	34	39	37	36	41	38	38	36	37	
Ab	11	11	13	14	11	13	14	10	10	15	14	18	18	19	21	25	23	8	13	15	
An	2	0	7	0	1	0	0	1	0	3	1	4	2	2	3	3	1	3	2	2	
Ну	7	10	10	9	6	7	8	10	7	7	5	8	5	8	10	4	7	7	9	8	
ASI	1.07	1.09	1.32	1.31	1.22	1.23	1.71	1.51	1.74	1.11	1.16	1.12	1.18	1.05	1.01	0.95	1.06	1.18	1.22	1.22	
H₂O by diff	7.36	2.79	7.88	8.21	4.24	5.62	7.8	9.38	7.41	3.83	2	2.24	2.47	5.36	2.51	0.93	0.43	2.95	6.72	4.74	
Mg#	0.22	0.18	0.2	0.38	0.17	0.16	0.27	0.3	0.27	0.26	0.18	0.24	0.24	0.2	0.19	0.21	0.21	0.21	0.37	0.23	
FeO+MgO+TiO ₂	4.95	5.69	5.08	4.42	4.51	4.17	4.09	5.24	3.8	3.51	2.84	4.36	3.02	4.66	5.46	2.56	4.34	4.67	4.79	4.32	
FeO+MgO	4.31	5.34	5.05	4.37	3.6	3.94	3.95	5.11	3.7	3.47	2.67	4.15	2.86	4.53	5.36	2.56	4.01	4.01	4.72	4.09	
K ₂ O/Na ₂ O	5.24	5.48	3.24	3.57	5.64	4.79	2.84	4.48	4.82	3.18	4.41	2.76	3.07	2.69	2.48	2.21	2.43	6.71	4.04	3.9	

Notes: Kerala Khondalite Belt, Southern India (KKB) and Barun gneiss, Himalaya (BAR) are from Ferrero et al. (2012). F16 = Oberpfalz migmatites from Ferrero et al. (2016a). AAV16 = Jubrique migmatites, Betic Cordillera (S Spain) from Acosta-Vigil et al. (2016). AAV07 = Grt+Bt granulitic enclaves of El Hoyazo, Neogene Volcanic Province (S Spain) from Acosta-Vigil et al. (2007). F11 = Spl-Crd granulitic enclaves of El Hoyazo from Ferrero et al. (2011). B13 = Sierra Alpujata metatexites, Betic Cordillera (S Spain) from Bartoli et al. (2013). (Table extends on next page.)

DISCUSSION

The present study targets polycrystalline inclusions in garnet form felsic granulites of the Central Maine Terrane. Our results confirm that they are volumes of crystallized melt trapped during garnet growth at the metamorphic peak, as already proposed based on mineralogical and microstructural investigation by Axler and Ague (2015). Raman investigation shows the presence of metastable cristobalite, i.e., formed outside its stability field (see e.g., Hwang et al. 2004). The occurrence of metastable polymorphs in nanogranitoids has been interpreted as direct evidence that the inclusions preserve their original composition, as these phases recrystallize to their most common counterparts (i.e., quartz) when the inclusions decrepitate, i.e., becomes an open system able to exchange components with the rock matrix via cracks in the host garnet (Ferrero et al. 2016b). Such inclusions, therefore, offer access to unaltered deep melts still preserved in the natural rock, which underwent melting at depth (Ferrero and Angel 2018).

The investigation of CMT nanogranitoids thus provides a detailed portrait of formation conditions, geochemistry, and volatile content of melt from metasediments at crustal depth. The extremely high *T* at which the melt was produced is close to the Bt-out curve according to the melting experiments on metasediments of Auzanneau et al. (2006). Indeed, the peraluminous and granitic nature of the re-homogenized melt, its relatively low amount of H₂O and its occurrence in (peritectic) garnet are all features consistent with melt generated by biotite dehydration melting (Le-Breton and Thompson 1988), with residual biotite

still locally visible as mineral inclusions (Fig. 1a). Furthermore, the enrichment in chlorine and fluorine of the trapped melt is likely to influence the stability of the biotite (see "Volatiles in high-pressure melt" section below).

The composition measured in the re-homogenized inclusions, especially its granitic character and the high-K/Na ratio (≈4:1) is consistent with the phase assemblage, which always includes quartz/cristobalite plus two K-bearing phases (muscovite and phlogopite). The phase 430 identified via Raman investigation is likely to be the "phase CV," reported in these inclusions by Axler and Ague (2015): the narrow peaks visible in its Raman spectrum show that it belongs to a crystalline phase. Moreover, very similar compositions to the one reported by Axler and Ague (2015) were measured in phase 430 from garnet pyroxenites from the Granulitgebirge (Bohemian Massif; unpublished EMP data; Ferrero et al. in preparation), thus making this phase the main Na repository in the targeted nanogranitoids. The K-rich

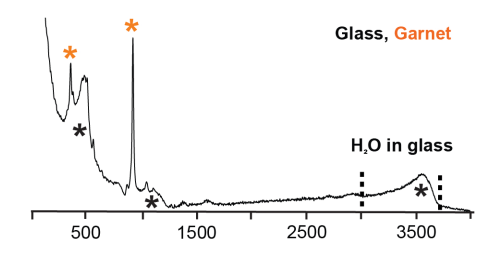


FIGURE 6. Raman spectrum of nanogranitoid re-homogenized to glass.

TABLE 2.—EXTENDED

	Expe	riments		Other nanogranitoids												
Name	P91	P91	KKB	St.dev.	BAR	St.dev.	F16	St.dev.	AV16	St.dev.	AV07	St.dev.	F11	St.dev.	B13	St.dev.
Duration			n = 11		n = 4		n = 4		n = 5		n = 62		n = 15		n = 15	
T (°C)	1025	1075	950		830		825		800		700		700		700	
P (GPa)	1.0	1.0	0.5		0.8		0.5		1.2/1.4		0.5		0.5		0.5	
wt%																
SiO ₂	70.62	69.44	73.96	(2.63)	73.77	(2.34)	70.78	(3.44)	70.16	(1.29)	71.23	(1.43)	68.95	(1.65)	70.03	(2.28)
TiO ₂	0.65	0.73	0.11	(0.09)	0.09	(80.0)	0.06	(0.05)	0.07	(0.06)	0.10	(0.03)	0.10	(0.12)	0.04	(0.07)
Al_2O_3	13.40	13.64	12.95	(1.31)	12.9	(1.46)	11.91	(0.68)	14.89	(0.98)	14.44	(0.33)	12.82	(1.14)	11.71	(0.86)
FeO	3.26	3.04	3.03	(0.69)	2.51	(0.37)	2.39	(0.76)	2.14	(0.59)	1.71	(0.52)	1.32	(0.40)	1.71	(0.21)
MnO	0.11	0.08	0.04	(0.03)	0.25	(0.17)	0.10	(0.10)	0.46	(0.07)	0.08	(0.05)	0.16	(0.17)	0.17	(0.10)
MgO	1.04	1.09	0.65	(0.21)	0.53	(0.13)	0.61	(0.07)	0.09	(0.02)	0.05	(0.04)	0.02	(0.03)	0.12	(0.07)
CaO	0.26	0.28	0.53	(0.20)	0.85	(0.48)	1.04	(0.56)	0.48	(0.13)	0.6	(0.09)	0.68	(0.16)	0.45	(0.13)
Na₂O	0.79	0.84	1.1	(0.32)	1.94	(0.13)	0.57	(0.45)	2.88	(1.24)	3.63	(0.39)	2.25	(0.35)	2.79	(0.35)
K₂O	5.98	6.05	6.72	(0.70)	4.86	(0.79)	6.24	(1.10)	3.97	(1.00)	4.97	(0.31)	4.56	(0.83)	4.05	(0.39)
P_2O_5	0.11	0.06	0.03	(0.05)	0.02	(0.02)	0.28	(0.09)	0.01	(0.01)	0.37	(0.09)	0.16	(0.07)	0.26	(0.23)
Cl	-	-	_		-		-		-		-		-		-	
Total	96.22	95.25	99.12		97.73		93.97		95.15		97.16		91.02		91.33	
Q	39	37	37		39		39		35		29		36		36	
C	5	5	3		3		3		5		3		3		3	
Or	35	36	40		29		37		23		29		27		24	
Ab	7	7	9		16		5		24		31		19		24	
An	1	1	2		4		3		2		1		2		1	
Ну	8	7	7		6		6		5		3		3		4	
ASI	1.63	1.62	1.29		1.29		1.24		1.50		1.16		1.30		1.19	
H₂O by diff	3.78	4.75	0.88		2.27		6.03		4.85		2.84		8.98		8.67	
Mg#	0.35	0.38	0.27		0.26		0.30		0.06		0.04		0.03		0.10	
FeO+MgO+TiO ₂	4.95	4.86	3.79		3.13		3.05		2.30		1.86		1.44		1.87	
FeO+MgO	4.30	4.13	3.68		3.04		2.99		2.23		1.76		1.34		1.83	
K ₂ O/Na ₂ O	7.57	7.20	6.09		2.51		11.01		1.38		1.37		2.02		1.45	

character of the melt has been previously observed in other nanogranitoid case studies (Cesare et al. 2009; Ferrero et al. 2012) and appears to be a typical feature of primary anatectic melts from metasediments melted at $T \ge 900$ °C (see Gianola et al. 2020 and related references).

A peculiarity of this case study is represented by the shape of the inclusions. Most case studies of nanogranitoids show inclusions with a more or less developed negative crystal shape, the response of host garnet to the need of lowering the surface free energy of the melt-garnet interface and move toward textural equilibration (Ferrero et al. 2012). Tubular/acicular shapes in nanogranitoids are not unheard of (Ferrero et al. 2012; Cesare et al. 2015), but they are overall a rarity. CMT nanogranitoids are a unique case as the acicular shape, i.e., defined by an extreme elongation/width ratio, characterizes the majority of the inclusions (Figs. 1b and 1c). So far, only the polycrystalline inclusions in the garnet megacrysts of Gore Mountain in the

TABLE 3. H_2O , CO_2 , and F contents in re-homogenized inclusions measured by NanoSIMS

Garnet	Analysis	H₂O	1σ	CO ₂	1σ	F	1σ
		(wt%)	error	(ppm)	error	(ppm)	error
1	Exp4_M1_1	4.38	0.05	5073	204	6820	106
	Exp4_M4_1	5.24	0.06	4979	201	3198	49
2	Exp4_M2_1	4.83	0.05	538	32	1033	15
	Exp4_M3_1	5.00	0.05	790	34	7223	112
3	Exp3_MI_2	3.93	0.05	603	34	541	8
	Exp3_MI_6	4.09	0.05	3983	164	5462	85
4	Exp3_MI_3	4.46	0.05	8109	339	535	8
	Exp3_MI_1	1.64	0.07	113	38	79	2
	Exp3_tub_1	3.85	0.05	504	32	479	7
	Exp3_1	4.18	0.17				
	Exp3_2	4.29	0.17				
5	Exp3_3	3.84	0.17				
	Exp3_4	4.69	0.17				

Adirondacks (Darling et al. 1997; Ferrero et al. 2021) show similar features, although in the latter case only \sim 50% of the inclusions have such shape (Ferrero and Angel 2018). Further investigations are needed to understand the reasons underlying the dichotomy negative-crystal vs. acicular shape in inclusions from different localities.

The original rationale for our work was twofold: verifying the former melt nature of the inclusions and obtaining the bulk composition of the original melt. The study however generated three most unexpected results: (1) re-homogenization experiments show that this melt formed under high-pressure (HP) conditions, in contrast with previous studies of these felsic granulites; (2) although the melt itself is peraluminous and granitic in composition, common features in melts from metasediments, it has an unexpectedly high-mafic (FeO+MgO) component; and (3) in terms of volatiles, the melt contains significant amounts of halogens (Cl, F) besides typical species observed in silicate melts, e.g., H₂O and CO₂.

First evidence of HP in the felsic granulites of the Central Maine Terrane

Possibly the most consequential result of our study is that the inclusions re-homogenize completely in equilibrium with the host garnet only at $P \ge 1.7$ GPa, considerably in excess of the minimum of 1.0 GPa inferred by Ague et al. (2013) and Axler and Ague (2015). Garnet growth conditions and thus MI entrapment coincide with those of partial melting, as both garnet and melt are products of the same melting reaction (Cesare et al. 2015 and references therein), and are under chemical equilibrium during their formation. Thus, successful re-homogenization experiments on nanogranitoids are a completely independent tool to constrain

American Mineralogist, vol. 106, 2021

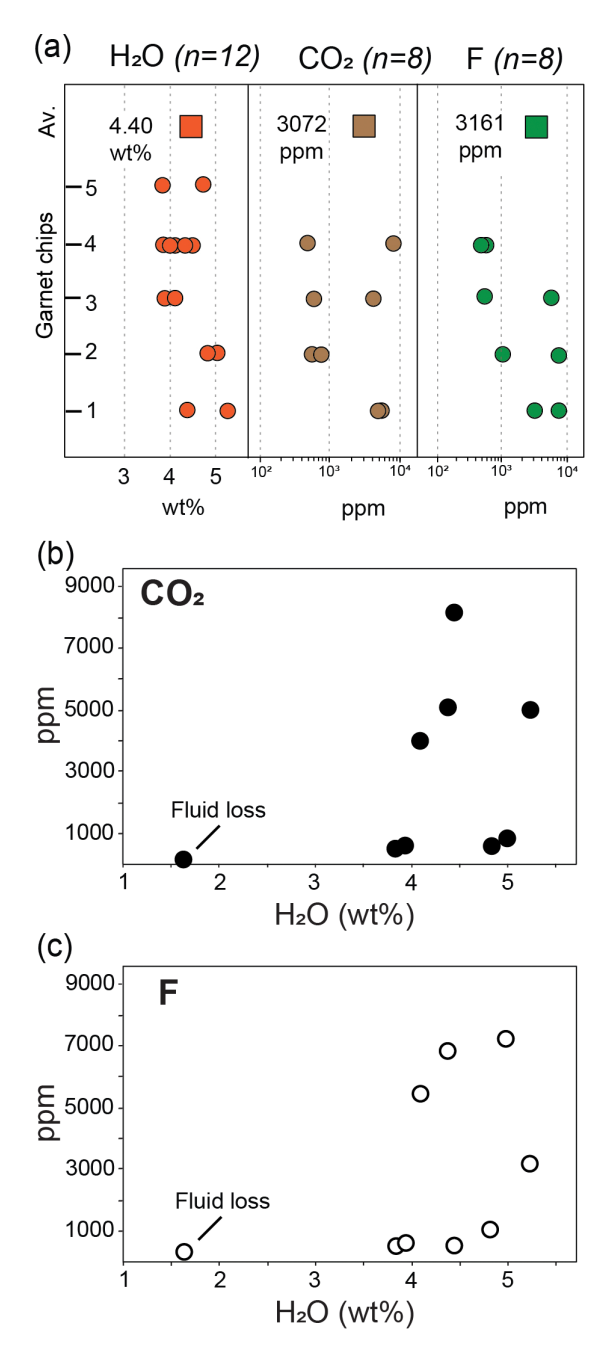


FIGURE 7. NanoSIMS measurements on re-homogenized nanogranitoids. (a) Measurements of H₂O, CO₂, and F presented according to the garnet chip in which they were measured. Variation diagrams of (b) CO₂ and (c) F with respect to H₂O for each single NanoSIMS analysis, including one inclusion with clear fluid loss (indicated in figure).

the P-T conditions of garnet formation in presence of melt (Ferrero et al. 2018b). Both P and T still need to be calculated beforehand using independent methods, e.g., thermodynamic modeling and classic geothermobarometry on the metamorphic assemblage to which the inclusion-bearing garnet belongs, to proceed with the experiments. If the calculated formation conditions are correct, (most of) the nanogranitoids should re-melt completely without

reacting with the host during the experimental run (Bartoli et al. 2013b; Acosta-Vigil et al. 2016). Conversely, textural evidence of melt-garnet disequilibrium, as well as decrepitation evidence, would indicate the experimental parameters were not representative of the formation conditions (Ferrero et al. 2018b; Ferri et al. 2020; Gianola et al. 2020). As an example, the critical evaluation of the nanogranitoid microstructures after heating experiments at different P allowed Ferrero et al. (2018b) to bracket the P conditions of melting of the felsic granulites of Orlica-Śnieżnik Dome (OSD; Bohemian Massif) to 2.7 ± 0.1 GPa, starting from an initial range of calculated P spanning from 1.8 to 3.0 GPa based on previous geothermobarometric and modeling studies.

Our detailed experimental work on the CMT nanogranitoids shows that the nanogranitoids re-melt at T = 1050 °C. At 1.0 GPa the abundance of decrepitation cracks in the re-melted inclusions is clear evidence of insufficient confining P, which leads to failure of the container (the garnet) due to inclusion overpressurization during the heating run. Moreover, all the experiments at P < 1.7 GPa show evidence of chemical disequilibrium between the newly produced glass and the surrounding garnet. This causes meltgarnet interaction, with formation of new phases not present in the inclusions before experimental runs, e.g., orthopyroxene and/or change in composition (Mg-increase) of the garnet around the inclusion. Newly formed, Mg-richer garnet was also reported in nanogranitoids from the OSD felsic granulites after experiments at P lower than those of melt formation (Ferrero et al. 2018b). Hence the microstructural appearance of the CMT nanogranitoids after reheating show an evolution similar to that reported in Ferrero et al. (2018b), with the Mg-rich garnet disappearing once the confining P reaches 1.7 GPa, thus demonstrating that both garnet and melt formed at $P \ge 1.7$ GPa.

High-mafic content in pristine anatectic melt from metasediments

Granitic melts with geochemistry similar to the CMT nanogranitoids, i.e., high-ASI index, high-normative orthoclase, and high FeO+MgO, are reported from experiments on natural metapelitic rocks at 1 GPa and 1025-1075 °C (Patiño Douce and Johnston 1991) and in nanogranitoid from metapelitic migmatites, which experienced UHT conditions, 950 °C and 0.5 GPa, in the Kerala Khondalite Belt, Southern India (Cesare et al. 2009; Ferrero et al. 2012) (see Table 2 and Figs. 8a and 8b for the whole nanogranitoid and experimental data set). It may be argued that such a mafic-rich character is the result of contamination between glass and host, as the inclusions are hosted in Fe- and Mg-rich garnet (Axler and Ague 2015). However, contamination via (even limited) dissolution of garnet during re-heating experiments can be excluded based on microstructural basis, i.e., the inclusions show regular shapes and completely lack embayments indicative of garnet dissolution. Contamination during EMP analysis can also be ruled out for the inclusions selected for EMP investigation and reported in Table 2. The size of the re-homogenized inclusions was sufficiently large (>5 μm in diameter) to avoid the excitation volume created by the electron beam (diameter 1 µm) to come in contact with the host. In the few cases where the inclusions were ≤5 μm, garnet contamination was clearly visible as the measured SiO₂ showed a sharp decrease, coupled with FeO increase (Fig. 8a). As microstructural evidence of garnet dissolution was completely absent from these small inclusions, we ascribed this phenomenon to the fact that the excitation volume created by the beam also included a portion of the host. Analyses from inclusions below 5 μ m were then removed from the data set (contaminated analyses are given in Online Material¹ Table OM1). Based on such considerations, the high-mafic component of the melt preserved in these felsic granulites should be considered a primary feature.

CMT nanogranitoids have a very high-FeO+MgO content when compared with experimental melts from metasedimentary protoliths, i.e., 2.58–5.64 wt% in the CMT nanogranitoids (on anhydrous basis) vs. 0.9–3.9 wt% of the experimental data set compiled by Stevens et al. (2007). The database of nanogranitoids and melt inclusions (Bartoli et al. 2016) shows that most of the melt inclusions (for a total of ~600 analyses in 2016) have a FeO+MgO+TiO₂ content in the range 0.25–2.50 wt%, with only ~10% of the whole database having contents 4–5 wt%. As CMT nanogranitoids show an average FeO+MgO+TiO₂ = 4.32 wt% (Table 2), their mafic component is higher than almost 90% of the anatectic melt inclusions measured so far.

Experimental work on Fe and Mg contents in haplogranitic melts (Johannes and Holtz 1996) and melting experiments on metasediments (Patiño Douce and Johnston 1991; Montel and Vielzeuf 1997; Droop et al. 2003) show that a granitic melt produced during melting of metasediments can accommodate a progressively higher amount of Fe and Mg as the formation T of the melt increases. Such observations, so far rooted exclusively in experimental findings, are now supported by our natural data. This is clearly visible when they are plotted against data available in the literature on granitic inclusions from metasediments melted at different T (Fig. 7; see also Table 2). Different case studies of nanogranitoids show a positive correlation between melting T (corresponding, in turn, to melt entrapment in the growing host) and FeO+MgO content. Indeed, the melt in the CMT nanogranitoids, which shows the highest FeO+MgO content among all the granitic inclusions, formed at $T \ge 1000$ °C, the highest formation T identified so far in nanogranitoids from metasediments. Conversely, the melt produced at lower T, 700–710 °C, shows the lowest FeO+MgO content, in the range 1.34–1.83 wt%.

Variable degrees of FeO+MgO enrichment are commonly

observed in leucosomes from partially melted metasediments and in S-type granites (Stevens et al. 2007; Villaros et al. 2009), commonly associated to an increase in A/CNK and a decrease in silica content (Taylor and Stevens 2010). This has been proposed to be the result of selective entrainment in the magma of peritectic garnet, the most common repository of Fe, Mg, and Al in metamorphosed crustal rocks, as the melt progressively coalesces at depth and migrates upward (Stevens et al. 2007). This hypothesis assumes that most pristine anatectic melts from metasediments are leucogranitic and very low in mafic components, a concept so far supported by both experiments (Stevens et al. 2007) and melt inclusions (Bartoli et al. 2016). However, our study demonstrates that anatectic melts can instead show a high content of Fe and Mg when produced at T > 1000 °C and, thus, they should be considered to have a pristine "starting" composition (Ferrero et al. 2012; Bartoli et al. 2016). This observation does not affect the validity of the peritectic phase entrainment hypothesis, which remains a sound explanation for FeO+MgO enrichment in S-type granites. It does, however, pose a significant caveat for researchers who want to correctly estimate the magnitude of peritectic phase entrainment experienced by the granitic body/leucosome under investigation, warning in particular against overestimating the magnitude of entrainment by assuming a too small FeO+MgO content in the original anatectic melt when the latter is produced at T in excess of 950–1000 °C.

Volatiles in high-pressure melt

 H_2O is necessary to stabilize any silicate melt under crustal conditions, and the quantification of H_2O , as well as of other species such as CO_2 and halogens, partitioned into deep partial melts, is of utmost importance for quantifying volatile cycles at depth and how they affect deep melting processes (Bartoli et al. 2014). NanoSIMS analyses on re-homogenized nanogranitoids is a routine approach in nanogranitoid studies (e.g., Acosta-Vigil et al. 2016), and it has shown that nanogranitoids generally preserve their original composition in terms of H_2O (Bartoli et al. 2014) and CO_2 contents (Carvalho et al. 2019). In particular, the loss of H_2O (even as OH) from the inclusion to the matrix surrounding the garnet would shift the liquidus of the trapped melt toward higher T (Johannes and Holtz 1996). Thus, the nanogranitoids

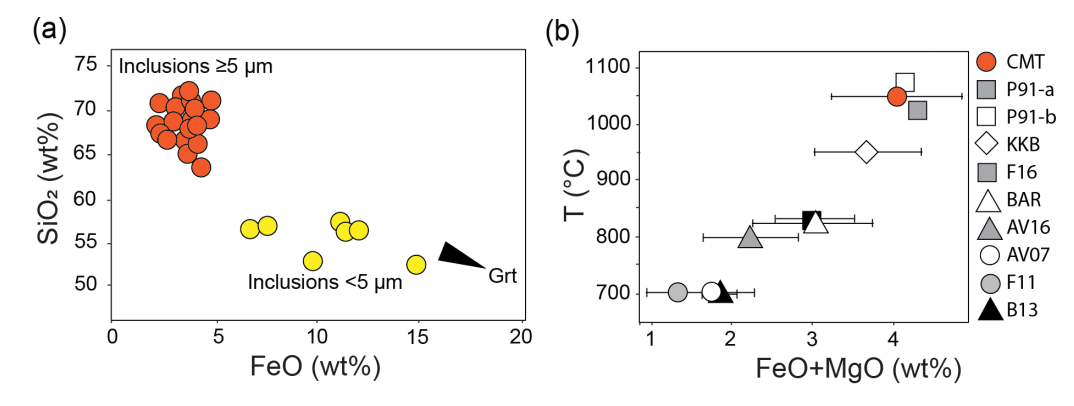


FIGURE 8. High-FeO+MgO content in re-homogenized CMT nanogranitoids. (a) Comparison between inclusion with diameter $\geq 5 \mu m$ (orange circles) and $\leq 5 \mu m$ (yellow circles; visible in Online Material¹ Table OM1). (b) FeO+MgO vs. *T* diagram, comparing nanogranitoids compositions from this study with previous case studies of inclusions in partially melted rocks with metasedimentary protolith (including standard deviations; data from Table 2). For abbreviations see caption Table 2.

would re-homogenize only at T significantly higher than those obtained via independent geothermobarometry on the host rocks, which is not the case here: the inclusions re-homogenize indeed at ~1050 °C, consistently with the T range of Zr-in-Rt thermometers on the rutile needles present in the nanogranitoid-bearing garnets (Axler and Ague 2015). In this work, the average H_2O value (4.40 wt%) is close to that obtained via difference from 100 of the EMP totals after alkali loss correction (4.74 wt%). Both values are consistent with experimental estimates of H_2O content in haplogranitic melts at the P-T conditions of interest, as the experimental parameters of the three successful experiments (points 3, 4, and 5 in Fig. 2) are close to the 4 wt% H_2O liquidus curve extrapolated at P >1.0 GPa (Johannes and Holtz 1996). Such values fit remarkably well also with the recent results of Makhluf et al. (2017) on granite formation at 1.0 GPa.

The melt also contains significant amounts of CO₂, on average ~3000 ppm (0.3 wt%). This CO₂ may be internally produced as a result of the devolatilization of hydrous silicates in the presence of graphite (Connolly and Cesare 1993; Cesare et al. 2005) visible in the CMT felsic granulites as trapped minerals in inclusions and/or as mineral inclusions in garnet and the rock matrix (Axler and Ague 2015). The CO₂ content of the CMT nanogranitoids is higher, on average, than in the nanogranitoids measured in the graphite-bearing metasediments of the Ivrea-Verbano Zone (IVZ; Carvalho et al. 2019). It is likely that the different depth at which melting occurred played a major role in shaping the CO₂ content of the melt. Experimental studies have shown that CO₂ solubility in melt increases dramatically with increasing $P(\sim 500 \text{ ppm} \text{ each})$ 0.1 GPa in experimental studies; Ni and Keppler 2013), and in fact our results show that CMT nanogranitoids likely formed at significantly greater depth than IVZ nanogranitoids, 1.7–2.0 GPa (this study) vs. 0.8 GPa (Carvalho et al. 2019).

Probably the most striking feature of the CMT melt is the presence of a significant amount of halogens. Cl (0.32 wt% average) and F (3161 ppm, or ~0.32 wt%) account together for 0.64 wt% on average of the total melt composition. This is also consistent with the fact that phlogopite crystallized inside the CMT nanogranitoids has been found, in one case, to contain an unusually high amount of F (>1 wt%; Axler and Ague 2015). Halogens are characteristic of brines, i.e., saline and Cl-rich fluid with low H2O activity, proposed by some authors to play an important role in the melting processes occurring in a thickened crust at either lower crustal or upper mantle conditions (Aranovich et al. 2014). The Cl content of partial melts can be used as proxy for the presence of brines during melt production at depth (Acosta-Vigil et al. 2016). CMT nanogranitoids contain 0.10-0.97 wt% of Cl, an amount comparable to those reported in experimental melts coexisting with brines, i.e., ranging between ~0.2 and 1.6 wt% (Webster and Mandeville 2007; Aranovich et al. 2013; Safonov et al. 2014).

Based on the extrapolation of existent experimental results on haplogranite melting in presence of $\rm H_2O$ -NaCl-KCl (750–950 °C/0.6–1.4 GPa; Aranovich et al. 2013), the brine originally present at >1000 °C and 2.0 GPa in the CMT granulites likely had $X_{\rm H_2O}$ ~0.3 (see Figs. 3 and 8 in Aranovich et al. 2013). More precise estimates are hampered by the lack of leftover fluid, i.e., primary fluid inclusions or detectable fluid in nanogranitoids, as well as of more precise experimental constraints, e.g., on CO₂- and

F-bearing systems at conditions closer to those of interest. Experiments show furthermore that brines in a haplogranitic system may cause a significant shift of the minimum melting T toward higher values due to the lowering of the H₂O activity (Aranovich et al. 2013). This would help to create the conditions for melting to occur at extreme $T(>1000 \,^{\circ}\text{C})$ as proposed for the CMT felsic granulites, a notion independently supported by both previous PT estimates (Ague et al. 2013; Axler and Ague 2015) as well as by the complete re-homogenization of the nanogranitoids at 1050 °C. Another possibility is that the enrichment in halogens predated the metamorphic peak, i.e., the brines were not present during melting but had infiltrated the felsic granulites during their prograde metamorphic evolution. In this scenario, Cl and F may be incorporated in the biotite, and this process extends biotite stability field toward UHT conditions (Kelsey and Hand 2015), thus allowing biotite to destabilize at significantly higher T than commonly expected.

IMPLICATIONS

The deep nature of granulite metamorphism and the highthermal flux required to achieve melting favor post-melting re-equilibration and re-crystallization of granulites/migmatites, often obliterating the most direct evidence of the presence of melt, such as leucosomes and melt pseudomorphs (White et al. 2011). For this reason, the preserved melt inclusions sheltered in peak peritectic garnet of the CMT felsic granulites are a crucial finding. They indeed provide new data necessary to create a more comprehensive portrait of the multiple aspects of melting, melt preservation, and crustal evolution during metamorphism in the deep roots of orogens. In particular, HP melts from metasediments are still underrepresented in the nanogranitoid database, as the bulk of the reported case studies are from rocks melted at $P \le 1.5$ GPa (see lists in Cesare et al. 2015; Bartoli et al. 2016; Acosta-Vigil et al. 2016; Ferrero et al. 2018b), with only one case at significantly greater depth >4.5 GPa (Stepanov et al. 2016). Our data are thus a step toward filling the gap in knowledge on natural partial melts forming at intermediate $P \sim 2.0$ GPa), along with the recent work on metasomatic nanogranitoids, originally from melting of crustal sedimentary rocks and now hosted in the Granulitgebirge pyroxenites (Borghini et al. 2018, 2020). A further important feature of the CMT nanogranitoids is the fact that they are richer in mafic components (FeO and MgO) than the majority of nanogranitoid case studies, regardless of the protolith. Their pristine nature thus provides a direct confirmation that the granitic melt from anatexis can accommodate an increasing amount of Fe and Mg with increasing T, an observation rooted until now exclusively in experimental studies. This finding is thus a caveat against assuming that natural pristine anatectic melts are always leucogranitic.

Our independent experimental results provide the first evidence of HP conditions during the metamorphic peak/melting of the felsic granulites in the Central Maine Terrane, pointing toward melting conditions of ~1050 °C and 1.7–2.0 GP. HP metamorphism, rather than purely UHT (Ague et al. 2013), is also supported by the widespread presence of pseudomorphs of sillimanite after kyanite in the matrix (Axler and Ague 2015). Our findings warrant a reappraisal of the metamorphic peak conditions in the area and finds direct support in other recent studies in nearby localities: HP conditions

(1.8 GPa) reported in silica-undersaturated gneisses (Keller and Ague 2018), whereas other metapelites contain evidence of UHP metamorphism (>5 GPa; Keller and Ague 2020). H₂O, CO₂, Cl, and F were measured directly in situ in the HP crustal melt still preserved in its original source rock. H₂O was previously measured in nanogranitoids from rocks equilibrated between ~0.4 and 1.4 GPa (Bartoli et al. 2014, 2016; Acosta-Vigil et al. 2016; Carvalho et al. 2019), whereas in situ CO₂ measurements are only available from the IVZ, metasediments equilibrated between 0.7 and 0.9 (Carvalho et al. 2019; Ferri et al. 2020; Gianola et al. 2021). Our new measurements extend the existing data set toward significantly greater depth and provide the foundation of further studies to further clarify how the interplay of protolith, fluid speciation, and P-T conditions influence H₂O and carbon budgets during crustal subduction and thickening. Moreover, to our knowledge, our study presents the first data on F measured in situ in anatectic melt inclusions. Previous experimental studies suggest that the presence of a significant amount of Cl, such as measured in the CMT inclusions, may be indicative of the presence of saline fluids (brines) during melting. This is the first direct natural evidence that brines infiltrating the lower crust as a metasomatic fluid may be an influential factor for the establishment of conditions necessary to produce melt at such extreme T (>1000 °C), commonly inferred to be characterized by fluid-absent melting conditions.

ACKNOWLEDGMENTS

Our deepest thanks go to C. Günter, F. Kaufmann, and L. Hecht for help during analyses and to C. Fischer for sample preparation. The authors are grateful to H. Lamadrid and an anonymous reviewer for their insightful comments that improved the quality of the paper and to M. Steele-McInnis for his careful editorial handling.

FUNDING

The present research was funded by the German Federal Ministry for Education and Research and the Deutsche Forschungsgemeinschaft (Project FE 1527/2-1 and FE 1527/2-2) to S.F. J.J. A gratefully acknowledges support from the National Science Foundation (EAR-1250269 and EAR-1753553) and Yale University. The NanoSIMS facility at the Muséum National d'Histoire Naturelle in Paris was established by funds from the CNRS, Région Ile de France, Ministère délégué à l'Enseignement supérieur et à la Recherche, and the Muséum National d'Histoire Naturelle.

REFERENCES CITED

- Acosta-Vigil, A., Cesare, B., London, D., and Morgan, G.B. VI (2007) Microstructures and composition of melt inclusions in a crustal anatectic environment, represented by metapelitic enclaves within El Hoyazo dacites, SE Spain. Chemical Geology 235, 450–465.
- Acosta-Vigil, A., Barich, A., Bartoli, O., Garrido, C.J., Cesare, B., Remusat, L., Poli, S., and Raepsaet, C. (2016) The composition of nanogranitoids in migmatites overlying the Ronda peridotites (Betic Cordillera, S Spain): The anatectic history of a polymetamorphic basement. Contributions to Mineralogy and Petrology, 171, 24.
- Ague, J.J., Eckert, J.O. Jr., Chu, X., Baxter, E.F., and Chamberlain, C.P. (2013) Discovery of ultrahigh-temperature metamorphism in the Acadian orogen, Connecticut, U.S.A. Geology, 41, 271–274.
- Aranovich, L.Y., Newton, R.C., and Manning, C.E. (2013) Brine-assisted anatexis: Experimental melting in the system haplogranite-H₂O-NaCl-KCl at deep-crustal conditions. Earth and Planetary Science Letters, 374, 111–120.
- Aranovich, L.Y., Makhluf, A.R., Manning, C.E., and Newton, R.C. (2014) Dehydration melting and the relationship between granites and granulites. Precambrian Research, 253, 26–37.
- Auzanneau, E., Vielzeuf, D., and Schmidt, M.W. (2006) Experimental evidence of decompression melting during exhumation of subducted continental crust. Contributions to Mineralogy and Petrology, 152, 125–148.
- Axler, J.A., and Ague, J.J. (2015) Oriented multiphase needles in garnet from ultrahigh-temperature granulites. American Mineralogist, 100, 2254–2271.
- Bartoli, O., Acosta-Vigil, A., Ferrero, S., and Cesare, B. (2016) Granitoid magmas preserved as melt inclusions in high-grade metamorphic rocks. American Mineralogist, 101, 1543–1559.
- Bartoli, O., Acosta-Vigil, A., Cesare, B., Remusat, L., Gonzalez-Cano, A., Wälle,

- M., Tačjmanová, L., and Langone, A. (2019) Geochemistry of Eocene-early Oligocene low-temperature crustal melts from Greater Himalayan Sequence (Nepal): a nanogranitoid perspective. Contributions to Mineralogy and Petrology, 174, 82.
- Bartoli, O., Česare, B., Poli, S., Acosta-Vigil, A., Esposito, R., Turina, A., Bodnar, R.J., Angel, R.J., and Hunter, J. (2013a) Nanogranite inclusions in migmatitic garnet: Behavior during piston cylinder re-melting experiments. Geofluids, 13, 405–420.
- Bartoli, O., Cesare, B., Poli, S., Bodnar, R.J., Acosta-Vigil, A., Frezzotti, M.L., and Meli, S. (2013b) Recovering the composition of melt and the fluid regime at the onset of crustal anatexis and S-type granite formation. Geology, 41, 115–118.
- Bartoli, O., Cesare, B., Remusat, L., Acosta-Vigil, A., and Poli, S. (2014) The H₂O content of granite embryos. Earth and Planetary Science Letters, 395, 281–290.
- Borghini, A., Ferrero, S., Wunder, B., Laurent, O., O'Brien, P.J., and Ziemann, M.A. (2018) Granitoid melt inclusions in orogenic peridotite and the origin of garnet clinopyroxenite. Geology, 46(11), 1007–1010.
- Borghini, A., Ferrero, S., O'Brien, P.J., Laurent, O., Günter, C., and Ziemann, M.A. (2020) Cryptic metasomatic agent measured in situ in Variscan mantle rocks: Melt inclusions in garnet of eclogite, Granulitgebirge, Germany. Journal of Metamorphic Geology, 38, 207–234.
- Brown, M. (2006) Duality of thermal regimes is the distinctive characteristic of plate tectonics since the Neoarchean. Geology, 34, 961–964.
- Bureau, H., Trocellier, P., Shaw, C., Khodja, H., Bolfan-Casanova, N., and Demouchy, S. (2003) Determination of the concentration of water dissolved in glasses and minerals using nuclear microprobe. Nuclear Instruments and Methods in Physics Research Section B: Beam Interactions with Materials and Atoms, 210, 449–454.
- Carvalho, B.B., Bartoli, O., Ferri, F., Cesare, B., Ferrero, S., Remusat, L., Capizzi, L.S., and Poli, S. (2019) Anatexis and fluid regime of the deep continental crust: New clues from melt and fluid inclusions in metapelitic migmatites from Ivrea Zone (NW Italy). Journal of Metamorphic Geology, 37(7), 951–975.
- Cesare, B., Meli, S., Nodari, L., and Russo, U. (2005) Fe³⁺ reduction during biotite melting in graphitic metapelites: another origin of CO₂ in granulites. Contributions to Mineralogy and Petrology, 149, 129–140.
- Cesare, B., Ferrero, S., Salvioli-Mariani, E., Pedron, D., and Cavallo, A. (2009) Nanogranite and glassy inclusions: the anatectic melt in migmatites and granulites. Geology, 37, 627–630.
- Cesare, B., Acosta-Vigil, A., Bartoli, O., and Ferrero, S. (2015) What can we learn from melt inclusions in migmatites and granulites? Lithos, 239, 186–216.
- Connolly, J.A.D., and Cesare, B. (1993) C-O-H-S fluid composition and oxygen fugacity in graphitic metapelites. Journal of Metamorphic Geology, 11, 368-378
- Créon, L., Levresse, G., Remusat, L., Bureau, H., and Carrasco-Núñez, G. (2018) New method for initial composition determination of crystallized silicate melt inclusions. Chemical Geology, 483, 162–173.
- Darling, R.S., Chou, I.-M., and Bodnar, R.J. (1997) An occurrence of metastable cristobalite in high-pressure garnet granulite. Science, 276, 91–93.
- Droop, G.T.R., Clemens, J.D., and Dalrymple, J. (2003) Processes and conditions during contact anatexis, melts escape and restite formation: The Huntly Gabbro complex, NE Scotland. Journal of Petrology, 44, 995–1029.
- Ferrero, S., and Angel, R.J. (2018) Micropetrology: Are inclusions in minerals grains of truth? Journal of Petrology, 59, 1671–1700.
- Ferrero, S., Bodnar, R.J., Cesare, B., and Viti, C. (2011) Reequilibration of primary fluid inclusions in peritectic garnet from metapelitic enclaves, El Hoyazo, Spain. Lithos, 124, 117–131.
- Ferrero, S., Bartoli, O., Cesare, B., Salvioli-Mariani, E., Acosta-Vigil, A., Cavallo, A., Groppo, C., and Battiston, S. (2012) Microstructures of melt inclusions in anatectic metasedimentary rocks. Journal of Metamorphic Geology, 30, 303–322
- Ferrero, S., Wunder, B., Walczak, K., Ziemann, M.A., and O'Brien, P.J. (2015) Preserved near ultrahigh-pressure melt from continental crust subducted to mantle depths. Geology, 43, 447–450.
- Ferrero, S., Wunder, B., Ziemann, Wälle, M., and O'Brien, P.J. (2016a) Carbonatitic and granitic melts produced under conditions of primary immiscibility during anatexis in the lower crust. Earth and Planetary Science Letters, 454, 121–131.
- Ferrero, S., Ziemann, M.A., Angel, R.J., O'Brien, P.J., and Wunder, P.J. (2016b) Kumdykolite, kokchetavite, and cristobalite crystallized in nanogranites from felsic granulites, Orlica Snieznik Dome (Bohemian Massif): Not evidence for ultrahigh pressure conditions. Contributions to Mineralogy and Petrology, 171, 3.
- Ferrero, S., Godard, G., Palmeri, R., Wunder, B., and Cesare, B. (2018a) Partial melting of ultramafic granulites from Dronning Maud Land, Antarctica: Constraints from melt inclusions and thermodynamic modelling. American Mineralogist, 103, 610–622.
- Ferrero, S., O'Brien, P.J., Borghini, A., Wunder, B., Wälle, M., Günter, C., and Ziemann, M.A. (2018b) A treasure chest full of nanogranitoids: an archive to investigate crustal melting in the Bohemian Massif. In S. Ferrero, P. Lanari, P. Goncalves, and E.G. Grosch, Eds., Metamorphic Geology: Microscale to mountain belts. Geological Society, London, Special Publications, 478, 13–38.Ferrero, S., Wannhoff, I., Laurent, O., Yakymchuk, C., Darling, R., Wunder, B.,

American Mineralogist, vol. 106, 2021

- Borghini, A., and O'Brien, P.J. (2021) Embryos of TTGs in Gore Mountain garnet megacrysts from water-fluxed melting of the lower crust. Earth and Planetary Science Letters, in press, https://doi.org/10.1016/j.epsl.2021.117058.
- Ferri, F., Cesare, B., Bartoli, O., Ferrero, S., Palmeri, R., Remusat, L., and Poli, S. (2020) Melt inclusions at MT. Edixon (Antarctica): Chemistry, petrology and implications for the evolution of the Lanterman range. Lithos, 374–375, 105685.
- Gianola, O., Bartoli, O., Ferri, F., Galli, A., Ferrero, S., Capizzi, L.S., Liebske, C., Remusat, L., Poli, S., and Cesare, B. (2021) Anatectic melt inclusions in ultra-high temperature granulites. Journal of Metamorphic Geology, in press.
- Hauri, E., Wang, J., Dixon, J.E., King, P.L., Mandeville, C., and Newman, S. (2002) SIMS analysis of volatiles in silicate glasses: 1. Calibration, matrix effects and comparisons with FTIR. Chemical Geology, 183, 99–114.
- Hwang, S-L., Shen, P., Chu, H-T., Yui, T-F, Liou, J-G., Sobolev, N.V., Zhang, R.Y., Shatsky, V.S., and Zayachkovsky, A.A. (2004) Kokchetavite: A new polymorph of KAlSi₃O₈ from the Kokchetav UHP terrain. Contributions to Mineralogy and Petrology, 148, 380–389.
- Johannes, W., and Holtz, F. (1996) Petrogenesis and experimental petrology of granitic rocks, 335 p. Berlin, Springer.
- Keller, D.S., and Ague, J.J. (2018) High-pressure granulite facies metamorphism (~1.8 GPa) revealed in silica-undersaturated garnet-spinel-corundum gneiss, Central Maine Terrane, Connecticut, U.S.A. American Mineralogist, 103, 1851–1868.
- ——— (2020) Quartz, mica, and amphibole exsolution from majoritic garnet reveals ultra-deep sediment subduction, Appalachian orogeny. Science Advances, 6, 11.
- Kelsey, D.E. (2008) On ultrahigh-temperature crustal metamorphism. Gondwana Research, 13, 1–29.
- Kelsey, D.E., and Hand, M. (2015) On ultrahigh temperature crustal metamorphism: Phase equilibria, trace element thermometry, bulk composition, heat sources, timescales and tectonic settings. Geoscience Frontiers, 6, 311–356.
- Le-Breton, N., and Thompson, A.B. (1988) Fluid-absent (dehydration) melting of biotite in metapelites in the early stages of crustal anatexis. Contributions to Mineralogy and Petrology, 99, 226–237.
- Makhluf, A.R., Newton, R.C., and Manning, C.E. (2017) Experimental determination of liquidus H₂O contents of haplogranite at deep-crustal conditions. Contributions to Mineralogy and Petrology, 172, 77.
- Mirwald, P.W., and Massonne, H.-J. (1980) Quartz-coesite transition and the comparative friction measurements in piston-cylinder apparatus using talc-alsimag glass (TAG) and NaCl high pressure cells: A discussion. Neues Jahrbuch für Mineralogie, 469–477.
- Montel, J.-M., and Vielzeuf, D. (1997) Partial melting of metagreywackes, Part II. Compositions of minerals and melts. Contributions to Mineralogy and Petrology, 128, 176–196.
- Morgan, G.B. VI, and London, D. (2005) Effect of current density on the electron microprobe analysis of alkali aluminosilicate glasses. American Mineralogist, 90, 1131–1138.
- Ni, H., and Keppler, H. (2013) Carbon in silicate melts. Reviews in Mineralogy and Geochemistry, 75, 251–287.
- O'Brien, P.J., and Ziemann, M.A. (2008) Preservation of coesite in exhumed eclogite: Insights from Raman mapping. European Journal of Mineralogy, 20, 827–834.
- Patiño Douce, A.E., and Johnston, A.D. (1991) Phase equilibria and melt productiv-

- ity in the pelitic system: implications for the origin of peraluminous granitoids and aluminous granulites. Contributions to Mineralogy and Petrology, 107, 202–218.
- Pownall, J.M., Armstrong, R.A., Williams, I.S., Thirlwall, M.F., Manning, C.J. and Hall, R. (2018) Miocene UHT granulites from Seram, eastern Indonesia: A geochronological–REE study of zircon, monazite and garnet. In S. Ferrero, P. Lanari, P. Goncalves, and E.G. Grosch, Eds., Metamorphic geology: Microscale to mountain belts. Geological Society, London, Special Publications, 478, 167–196.
- Safonov, O.G., Kosova, S.A., and van Reenen, D.D. (2014) Interaction of biotite-amphibole gneiss with H₂O-CO₂-(K, Na)Cl fluids at 550 MPa and 750 and 800 °C: Experimental study and applications to dehydration and partial melting in the middle crust. Journal of Petrology, 55, 2419–2456.
- Stepanov, A.S., Hermann, J., Rubatto, D., Korsakov, A.V., and Danyushevsky, L.V. (2016) Melting History of an ultrahigh-pressure paragneiss revealed by multiphase solid inclusions in garnet, Kokchetav Massif, Kazakhstan. Journal of Petrology, 57, 1531–1554.
- Stevens, G., Villaros, A., and Moyen, J.-F. (2007) Selective peritectic garnet entrainment as the origin of geochemical diversity in S-type granites. Geology, 35, 9–12.
- Taylor, J., and Stevens, G. (2010) Selective entrainment of peritectic garnet into S-type granitic magmas: Evidence from Archaean mid-crustal anatectites. Lithos. 120, 277–292.
- Thomen, A., Robert, F., and Remusat, L. (2014) Determination of the nitrogen abundance in organic materials by NanoSIMS quantitative imaging. Journal of Analytical Atomic Spectrometry, 29, 512–519.
- Tomkins, H.S., Powell, R., and Ellis, D.J. (2007) The pressure dependence of the zirconium-in-rutile thermometer. Journal of Metamorphic Geology, 25, 703-713.
- Villaros, A., Stevens, G., Moyen, J.F., and Buick, I.S. (2009) The trace element compositions of S-type granites: Evidence for disequilibrium melting and accessory phase entrainment in the source. Contributions to Mineralogy and Petrology, 158, 543–561.
- Webster, J.D., and Mandeville, C.W. (2007) Fluid immiscibility in volcanic environments. In A. Liebscher and C.A. Heinrich, Eds., Fluid-Fluid Interactions. Reviews in Mineralogy and Geochemistry, 65, 313–362.
- White, R.W., Stevens, G., and Johnson, T.E. (2011) Is the crucible reproducible? Reconciling melting experiments with thermodynamic calculations. Elements, 7, 241–246.
- Whitney, D.L., and Evans, B.W. (2010) Abbreviations for names of rock-forming minerals. American Mineralogist, 95, 185–187.

Manuscript received June 29, 2020 Manuscript accepted October 7, 2020 Manuscript handled by Matthew Steele-MacInnis

Endnote:

¹Deposit item AM-21-87690, Online Material. Deposit items are free to all readers and found on the MSA website, via the specific issue's Table of Contents (go to http://www.minsocam.org/MSA/AmMin/TOC/2021/Aug2021_data/Aug2021_data.html).